

Ferromagnetic Ising model on the hierarchical pentagon lattice

Takumi Oshima¹, and Tomotoshi Nishino^{2*}

¹Department of Physics, Faculty of Science, Kobe University, Kobe 657-8501, Japan

²Department of Physics, Graduate School of Science, Kobe University, Kobe 657-8501, Japan

Thermodynamic properties of the ferromagnetic Ising model on the hierarchical pentagon lattice is studied by means of the tensor network methods. The lattice consists of pentagons, where 3 or 4 of them meet at each vertex. Correlation functions on the surface of the system up to $n = 10$ layers are evaluated by means of the time evolving block decimation (TEBD) method, and the power law decay is observed in the high temperature region. The recursive structure of the lattice enables complementary numerical study for larger systems, by means of a variant of the corner transfer matrix renormalization group (CTMRG) method. Calculated spin expectation value shows that there is a mean-field type order-disorder transition at $T_1 = 1.58$ on the surface of the system. On the other hand, the bulk part exhibits the transition at $T_2 = 2.269$. Consistency of these calculated results is examined.

arXiv:2403.15829v1 [cond-mat.stat-mech] 23 Mar 2024

1. Introduction

The order-disorder phase transition has been one of the central concerns in modern statistical physics.¹⁾ The Ising model²⁾ has been extensively studied as a theoretical model of magnetic materials that consists of locally interacting molecular magnetic moments.³⁾ On the square lattice, presence of the phase transition was proven by Peierls,⁴⁾ and the exact formula for the free energy in the thermodynamic limit was later obtained by Onsager.⁵⁾ The concept of the renormalization group (RG) provides the unified picture on the singular behavior of thermodynamic functions around the phase transition point.⁶⁻⁸⁾ The nature of the second-order phase transition on the regular lattice that can be uniformly drawn on the *flat plane* is well understood from the view point of the conformal field theory.⁹⁾

The Ising model on the Cayley tree lattices has been known as a reference model, where the partition function of the whole system can be easily obtained by taking spin configuration sum from the boundary sites.¹⁰⁾ Although the corresponding free energy is an analytic function of the temperature T , those bulk spins deep inside the system, which are around the root of the tree, can possess finite spontaneous magnetic moment below the transition temperature, under the presence of infinitesimally weak external field.¹¹⁻¹³⁾ The transition is mean-field like, as it is explained from the self-consistent study on the Bethe lattice.^{10,14)}

Similarly, on the hyperbolic $(5, 4)$ lattice, where four pentagons meet at each vertex, presence of the mean-field like phase transition in the bulk part of the system was confirmed numerically for the ferromagnetic Ising model by means of the corner transfer matrix renormalization group (CTMRG) method¹⁵⁻¹⁹⁾ adapted to the hyperbolic lattice structure.^{20,21)} Since the $(5, 4)$ lattice is a regular lattice on the *negatively curved surface*, which has a finite curvature radius R as the typical length scale, the bulk part of the system cannot be critical, where there is scale invariance.²²⁾ Thus the correlation length of the model (along the geodesics) is always finite, even at the bulk transition temperature.²³⁾ It is naturally expected that ferromagnetic Ising models on the hyperbolic

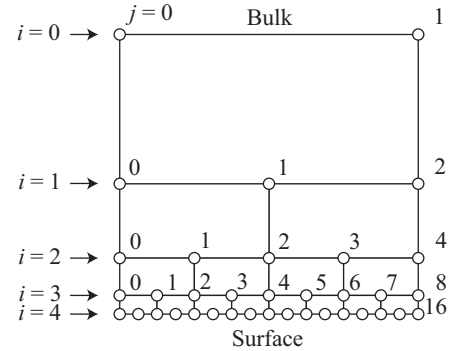


Fig. 1. Structure of the hierarchical pentagon lattice in the case $n = 4$. We regard σ_0^0 and σ_1^0 at the top as the *bulk* spins, and those σ_j^4 from $j = 0$ to $j = m(4) = 16$ at the bottom as the *surface* spins.

(p, q) lattices, where q numbers of p -gons meet at the lattice point, share the mean-field nature.²⁴⁾

Recently, Asaduzzaman et al performed the Monte Carlo simulation for the Ising model on the hyperbolic $(3, 7)$ lattice.²⁵⁾ From the numerical study on finite size systems, they confirmed presence of the power-law decay of the correlation function on the boundary of the system at any temperature. Okunishi and Takayanagi have rigorously shown the power-law decay along the boundary of the trivalent Cayley tree lattice,²⁶⁾ which is the hyperbolic $(\infty, 3)$ lattice, and reinterpreted the system from the view point of the Ads/CFT correspondence.²⁷⁻³⁰⁾ One of the theoretical interests on the hyperbolic (p, q) lattice is to confirm the presence, or absence, of the order-disorder transition at the system boundary.

Motivated from these recent studies focused on the hyperbolic lattices, in this article we analyze the thermodynamic properties of the ferromagnetic Ising model on the hierarchical *pentagon* lattice shown in Fig. 1. Typically the case when there are $n = 4$ layers of horizontally aligned pentagons is drawn. It should be noted that all the pentagons are represented by the rectangular shape, so that the hierarchical lattice structure can be captured systematically. There are $2^n - 1$ pentagons in total. Three or four pentagons meet on each vertex, and the number is exceptionally 2 at the system boundary.

*nishino@kobe-u.ac.jp

There is an Ising spin $\sigma_j^i = \pm 1$ shown by the open circle on each vertex, where the index i specifies the row from the top $i = 0$ to the bottom $i = n$, and where j specifies the horizontal location from the left $j = 0$ to the right $j = 2^i$. In order not to use nested index in the following equations, we introduce the notation $m(i) = 2^i$, where $m(i) + 1$ is the number of sites on the i -th row. The lattice has a geometrical analogy with the Cayley tree, in the sense that we obtain the binary tree by connecting the centers of vertically touching pentagons. Thus the upper boundary of the lattice with $i = 0$ corresponds to the root of the tree, and the lower boundary with $i = n$ corresponds to the leaves. Considering the analogy, we regard σ_0^0 and σ_1^0 at the top as the *bulk* spins, and σ_j^n for arbitrary j at the bottom as the *surface* spins.

Pairwise Ising interaction is present between each neighboring spins connected by the line. The Hamiltonian of the system is given by

$$H_n(\{\sigma\}) = -J \sum_{i=0}^{n-1} \sum_{j=0}^{m(i)-1} \sigma_j^i \sigma_{j+1}^i - J \sum_{i=0}^{n-1} \sum_{j=0}^{m(i)} \sigma_j^i \sigma_{2j}^{i+1}, \quad (1)$$

where $J > 0$ is the ferromagnetic coupling constant. In the left hand side, all the spins contained in the system is shortly denoted by $\{\sigma\}$. We assume that there is no external magnetic field, unless otherwise noted. The thermodynamic properties of the system can be obtained from the partition function

$$Z_n(T) = \sum_{\{\sigma\}} \exp \left[-\frac{H_n(\{\sigma\})}{k_B T} \right], \quad (2)$$

where T is the temperature, and where k_B is the Boltzmann constant. We set the temperature unit so that $k_B = 1$ is satisfied. The sum of the Boltzmann weight of the whole system is taken for all the possible spin configurations.

In this article, we perform numerical study on the system by the time evolving block decimation (TEBD) method^{31,32} up to the case $n = 10$, and complementary by the modified CTMRG method for larger systems. We show that the surface spin expectation value at the center of the n -th row $\langle \sigma_{m(n)/2}^n \rangle$ is non-zero below $T_1 = 1.58$, when n is sufficiently large. On the other hand, the bulk spin expectation value $\langle \sigma_0^0 \rangle = \langle \sigma_1^0 \rangle$ becomes non-zero from higher temperature $T_2 = 2.269$. When T is larger than T_1 , the correlation function along the surface row shows power-law decay.

The structure of this article is as follows. In Sec. II, we shortly explain the way how to apply TEBD method, and show the calculated entanglement entropy and the correlation function. In Sec. III we explain the numerical algorithm of the modified CTMRG method, which is complementary used for thermodynamic analysis, and show the calculated numerical results. Conclusions are summarized in the last section, and the remaining problems are discussed.

2. Application of the TEBD Method

In this section we explain how to perform the thermodynamic study on the Ising model on the hierarchical pentagon lattice, by means of the TEBD method. Let us consider the probability distribution function

$$G_n(\sigma_0^n, \dots, \sigma_{m(n)}^n) = \sum_{\{\sigma^0\}} \dots \sum_{\{\sigma^{n-1}\}} \exp \left[-\frac{H_n(\{\sigma\})}{k_B T} \right] \quad (3)$$

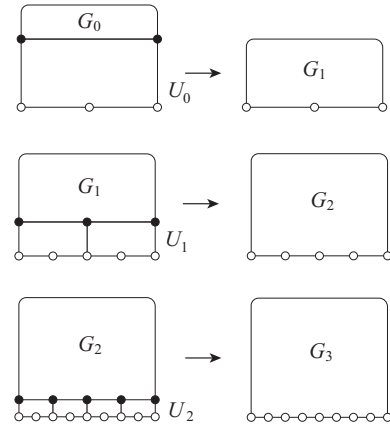


Fig. 2. Pictorial representation of the transfer matrix multiplications in Eq. (5) from $i = 0$ to $i = 2$.

at the bottom boundary. The configuration sum is taken for those row spins $\sigma_0^i, \dots, \sigma_{m(i)}^i$, which are shortly denoted by $\{\sigma^i\}$, from $i = 0$ to $i = n - 1$. The left hand side can be written in the short form $G_n(\{\sigma^n\})$. Introducing the transfer matrix

$$\begin{aligned} U_i(\{\sigma^{i+1}\} | \{\sigma^i\}) &= U_i(\sigma_0^{i+1}, \dots, \sigma_{m(i+1)}^{i+1} | \sigma_0^i, \dots, \sigma_{m(i)}^i) \\ &= \exp \left[\frac{J}{k_B T} \sum_{j=0}^{m(i+1)-1} \sigma_j^{i+1} \sigma_{j+1}^{i+1} + \frac{J}{k_B T} \sum_{j=0}^{m(i)} \sigma_j^i \sigma_{2j}^{i+1} \right], \quad (4) \end{aligned}$$

we can obtain the distribution function in Eq. (3) by way of the successive multiplication of the transfer matrix

$$G_{i+1}(\{\sigma^{i+1}\}) = \sum_{\{\sigma^i\}} U_i(\{\sigma^{i+1}\} | \{\sigma^i\}) G_i(\{\sigma^i\}), \quad (5)$$

starting from the initial distribution

$$G_0(\sigma_0^0, \sigma_1^0) = \exp \left[\frac{J}{k_B T} \sigma_0^0 \sigma_1^0 \right] \quad (6)$$

at the top of the system. Figure 2 shows the pictorial representation of the transfer matrix multiplication in Eq. (5) from $n = 0$ to $n = 2$. Configuration sums are taken for the spins shown by the black dots. Since $G_n(\{\sigma^n\})$ is the function of $m(n) + 1 = 2^n + 1$ number of the surface spins $\{\sigma^n\}$, direct numerical calculation can be performed only up to several layers, around $n = 5$ or $n = 6$.

If we regard $G_n(\{\sigma^n\})$ as the quantum amplitude, the corresponding quantum state is expected to be weakly entangled, since the lattice can be horizontally separated by cutting only $n + 1$ horizontal bonds along the vertical cut, similar to the multi-scale entanglement renormalization Ansatz (MERA) network.^{33,34} Thus $G_n(\{\sigma^n\})$ could be precisely represented by means of the matrix product state (MPS).^{35,36} Since the transfer matrix in Eq. (4) consists of horizontal product of local factors, the transfer matrix multiplication in Eq. (5) can be efficiently performed step by step by means of the TEBD method.^{31,32}

We explain some details in the numerical transfer matrix multiplication, when the distribution function is represented in the form of MPS. Those readers who are not interested in specific computational procedures can skip to the next subsection. In order to simplify the mathematical notations, we represent the Ising spins and corresponding tensor legs simply

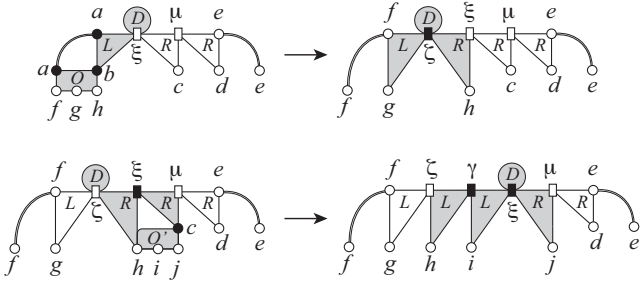


Fig. 3. Pictorial representation of the multiplication of U_2 to G_2 part by part, drawn by the IRF-type diagram. At the left and the right ends of the diagram, the spins connected by the arc are the same.

by alphabets, when the abbreviation is necessary.³⁷⁾ Suppose that we have the distribution function G_2 in the form of the mixed canonical MPS

$$G_2(abcde) = \sum_{\xi\mu} L_b^{a\xi} D^\xi R_c^{\xi\mu} R_d^{\mu e}, \quad (7)$$

where we have expressed the row spin $\sigma_0^2, \sigma_1^2, \sigma_2^2, \sigma_3^2, \sigma_4^2$ simply by $abcde$. The 3-leg tensors $L_b^{a\xi}$, $R_c^{\xi\mu}$ and $R_d^{\mu e}$ satisfies the orthogonality^{35,36)}

$$\begin{aligned} \sum_{ab} L_b^{a\xi} L_b^{a\xi'} &= \delta_{\xi\xi'}, \\ \sum_{\mu c} R_c^{\xi\mu} R_c^{\xi'\mu} &= \delta_{\xi\xi'}, \\ \sum_{de} R_d^{\mu e} R_d^{\mu' e} &= \delta_{\mu\mu'}, \end{aligned} \quad (8)$$

and D^ξ represents the singular value. In order to naturally arrange the spin indices in the equations, we put auxiliary indices on the upside of each tensors. Since all the tensor elements are real valued, we do not have to care about the complex conjugate. Hereafter we distinguish the 3-leg tensors and singular values by their indices.

In the process of obtaining G_3 by multiplying U_2 to G_2 , we perform the calculation part by part from left to right. We first prepare the 5-leg tensor

$$O_{fgh}^{a b} = \exp\left[\frac{J}{k_B T}(af + fg + gh + hb)\right], \quad (9)$$

which is a local factor contained in U_2 , and perform the contraction with $L_b^{a\xi} D^\xi$ in the manner

$$X_{fgh}^{\xi} = \sum_{ab} O_{fgh}^{a b} L_b^{a\xi} D^\xi. \quad (10)$$

We then perform the singular value decomposition (SVD) on X_{fgh}^{ξ} , grouping the tensor legs to fg and $h\xi$, to obtain the decomposed form

$$X_{fgh}^{\xi} = \sum_{\zeta} L_g^{f\zeta} D^\zeta R_h^{\zeta\xi}. \quad (11)$$

These local contraction and SVD processes are pictorially shown in the upper part of Fig. 3, where the whole part of the MPS is drawn in the form of the interaction round a face (IRF) type tensor-network diagrams.³⁸⁾

The next piece we multiply is the 4-leg tensor

$$O'_{hij}{}^c = \exp\left[\frac{J}{k_B T}(hi + ij + jc)\right], \quad (12)$$

and we take the contraction in the manner

$$Y_{hij}^{\zeta\mu} = \sum_{\xi c} O'_{hij}{}^c D^\xi R_h^{\zeta\xi} R_c^{\xi\mu}. \quad (13)$$

This time we perform the SVD to $Y_{hij}^{\zeta\mu}$ twice, and obtain the canonically decomposed form

$$Y_{hij}^{\zeta\mu} = \sum_{\gamma\xi} L_h^{\zeta\gamma} L_i^{\gamma\xi} D^\xi R_j^{\xi\mu}. \quad (14)$$

These processes are pictorially shown in the lower part of Fig. 3. In this manner, we can proceed to the next contraction with $O'_{jkl}{}^d$ and the following SVD, and also to the final contraction with $O'_{lmn}{}^e$ and the following SVD, to complete the transfer matrix multiplication $G_3 = U_2 G_2$. We finally obtain the MPS representation

$$G_3(fghijklmn) = \sum_{\zeta\gamma\xi\mu\nu\rho} L_g^{f\zeta} L_h^{\zeta\gamma} L_i^{\gamma\xi} L_j^{\xi\mu} L_k^{\mu\nu} L_l^{\nu\rho} D^\rho R_m^{\rho n} \quad (15)$$

of G_3 , where D^ρ is located in the right side. Every time we perform SVD, we normalize the singular values so that their sum is unity. Thus in Eq. (15),

$$\sum_{\rho} D^\rho = 1 \quad (16)$$

is satisfied in after the normalization. In the case we need $Z_n(T)$, we store the normalization constant somewhere. It is convenient to move the singular value back to the left side, by means of successive reorthogonalization, in order to start the next multiplication $G_4 = U_3 G_3$ in the same manner as Eqs. (9)-(16).

It seems that the degree of freedom for $\zeta, \gamma, \xi, \mu, \nu$, and ρ in Eq. (15) should be 4, 8, 16, 16, 8, and 4 for the exact MPS representation of G_3 , but actually the necessary singular values are less than those. Because of the lattice structure of the hierarchical pentagon lattice, the rank of G_3 when it is regarded as a matrix with respect to a bipartition of the spin row $fghijklmn$ is smaller than that is expected from the matrix size. Such a low-rank property is common in G_n for arbitrary n . Actually, it is not necessary to keep large number of singular values in the numerical calculation, since G_n is only weakly entangled by the construction of the lattice.

2.1 Calculated Results by the TEBD Method

We calculated the distribution function $G_n(\sigma_0^n, \dots, \sigma_{m(n)}^n)$ up to $n = 10$ by means of the TEBD method. The number of the kept singular values χ is automatically determined, so that the sum of the discarded singular values do not exceed the cut off parameter ε , where we vary it from $\varepsilon = 10^{-5}$ to $\varepsilon = 10^{-8}$ to confirm the numerical convergence of the obtained results. Hereafter we consider the case where the Ising interaction parameter J in Eq. (1) is unity.

We first focus on the division of the surface spin row $\{\sigma^n\}$ to the left half $\sigma_0^n, \dots, \sigma_{m(n)/2}^n$ and the right half $\sigma_{m(n)/2+1}^n, \dots, \sigma_{m(n)}^n$, and calculate the corresponding entan-

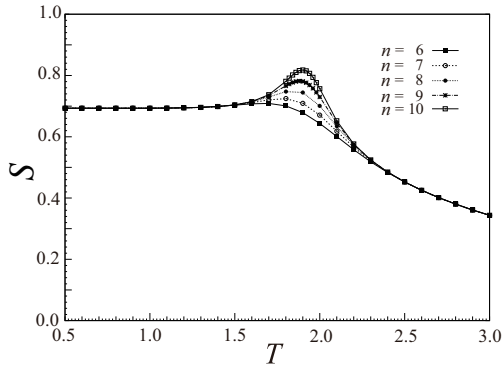


Fig. 4. Temperature dependence of the Entanglement entropy $S(T)$ in Eq. (17). Curves are guide to eye.

glement entropy (EE)

$$S(T) = - \sum_{\kappa} D^{\kappa} \ln D^{\kappa}, \quad (17)$$

where D^{κ} denotes the normalized singular value located between $\sigma_{m(n)/2}^n$ and $\sigma_{m(n)/2+1}^n$, when G_n is represented in the form of MPS. Figure 4 shows the temperature dependence of $S(T)$ in the cases $n = 6, 7, 8, 9$, and 10 . In low temperature we have $S(T) = \ln 2$, which corresponds to the *superposition* of the complete ferromagnetic state, and in high temperature $S(T)$ monotonously decreases with T . There is a peak structure in the region $1.5 < T < 2.4$, where n -dependence of $S(T)$ is visible. The peak height almost linearly increases with n , and it can be conjectured that $S(T)$ has a sharp peak at some temperature, where phase transition occur, in the thermodynamic limit $n \rightarrow \infty$.

Next, let us observe the correlation function on the surface $\{\sigma^{n=10}\}$. Figure 5 shows the correlation function $\langle \sigma_{m(10)/2-\ell/2}^{10} \sigma_{m(10)/2+\ell/2}^{10} \rangle = \langle \sigma_{512-\ell/2}^{10} \sigma_{512+\ell/2}^{10} \rangle$ with respect to the distance ℓ , calculated in high temperature region where $S(T)$ is converged with respect to n . As shown in the figure, power law decays with ℓ are observed, although there are minor fluctuation that arises from the inhomogeneous effect from the upper layers to the surface spin row. The presence of the power-law decay is in accordance with the Monte Carlo study by Asaduzzaman et. al. performed on finite hyperbolic (3, 7) disks.²⁵⁾

3. Application of the Modified CTMRG Method

Complementary to the TEBD method, we introduce the modified CTMRG method, which can be used for the evaluation of the partition function $Z_n(T)$ in Eq. (2) and spin expectation values, such as $\langle \sigma_0^0 \rangle$, $\langle \sigma_1^0 \rangle$, and $\langle \sigma_{m(n)/2}^n \rangle$, even when n is relatively large. Those readers who are not interested in the numerical algorithm can skip to the next subsection.

The Boltzmann weight of the whole system, which appears in the r.h.s. of Eqs. (2)-(3), can be represented as the product of the IRF weight W_{cde}^{ab} and the boundary weight B_{fg} , which are pictorially shown in Fig. 6. We use the IRF representation, since it is easy to treat Ising spins directly under the context of the (modified) CTMRG method.^{10,16)} The IRF weight is given by

$$W_{cde}^{ab} = \exp \left[\frac{J}{2k_B T} (ac + cd + de + eb + ba) \right], \quad (18)$$

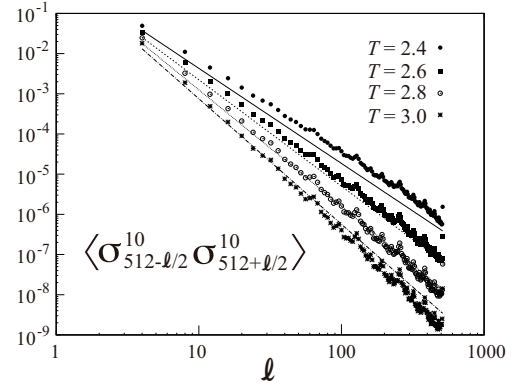


Fig. 5. Correlation function $\langle \sigma_{512-\ell/2}^{10} \sigma_{512+\ell/2}^{10} \rangle$ on the surface at $T = 2.4, 2.6, 2.8$, and 3.0 . Lines denote the decay estimated from $\langle \sigma_0^n \sigma_{m(n)}^n \rangle$ calculated by the modified CTMRG method through Eqs. (33)-(35), for the corresponding temperatures.

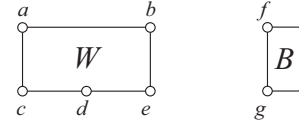


Fig. 6. Pictorial representation of the IRF weight W_{cde}^{ab} in Eq. (18), and the boundary weight B_{fg} in Eq. (19).

where a, b, c, d , and e represent the Ising spins on each vertex of the pentagon. Since each bond other than that on the system boundary is shared by adjacent pentagons, the parameter J is divided by 2 in the right hand side. Additionally we introduce the boundary weight

$$B_{fg} = \exp \left[\frac{J}{2k_B T} f g \right], \quad (19)$$

in order to adjust the Boltzmann weight at the boundary of the system. Let us use the notation B_g^f for the vertical boundary. In the case of the lattice with $n = 4$ in Fig. 1, there are $2^n - 1 = 15$ IRF weights, $2n = 8$ vertical boundary weights, and $2^n + 1 = 17$ horizontal ones.

In the CTMRG formulation, the whole system is divided into several components, and the Boltzmann weight for each component is calculated through the recursive area extensions and renormalization group transformations.¹⁵⁻¹⁹⁾ One of such weights on the hierarchical pentagon lattice are the series of the half-column transfer matrices (HCTM), which are located around the bottom of the system. The smallest one is given by

$$P_{0\ ce}^{ab} = \sum_d W_{cde}^{ab} B_{cd} B_{de}, \quad (20)$$

where the position of the spins are shown in the upper side of Fig. 7. Boundary weights B_{cd} and B_{de} are multiplied, since c, d , and e are spins on the bottom boundary, which is the surface. By definition, the HCTM satisfies the left-right symmetry $P_{0\ ce}^{ab} = P_{0\ ec}^{ba}$. Another series of the weights are the corner transfer matrices (CTM), which are located around the bottom left or the bottom right corners of the system. The smallest

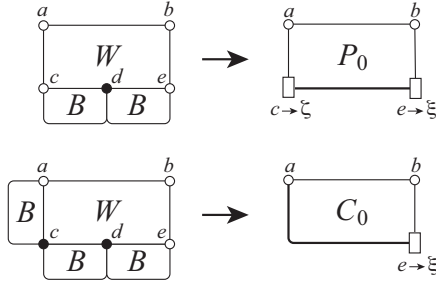


Fig. 7. The smallest HCTM $P_{0\zeta\xi}^{ab}$ in Eq. (20) and the CTM $C_{0\xi}^{ab}$ in Eq. (21), which are located around the bottom of the system. Those contracted tensor legs are shown by the filled marks.

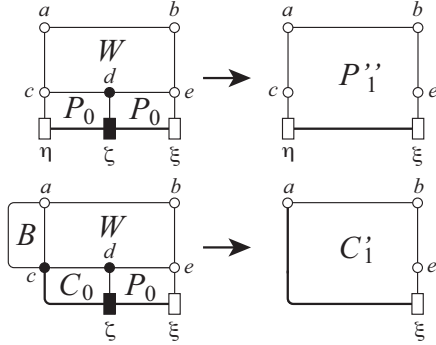


Fig. 8. The extension process of the HCTM in Eq. (23), and that of the CTM in Eq. (24).

one around the bottom left is expressed as

$$C_{0e}^{ab} = \sum_{cd} B_c^a W_{cde}^{ab} B_{cd} B_{de} = \sum_c B_c^a P_{0ce}^{ab}, \quad (21)$$

and similarly the one around the bottom right as

$$C_{0c}^{ab} = \sum_{de} W_{cde}^{ab} B_{cd} B_{de} B_e^b = \sum_e P_{0ce}^{ab} B_e^b. \quad (22)$$

For the latter convenience, let us use greek letters for those spins on the surface, in the manner as $P_{0\zeta\xi}^{ab}$, $C_{0\xi}^{ab}$ and $C_{0\zeta}^{ab}$.

The recursive structure of the hierarchical pentagon lattice enables the systematic extension of the HCTM. Taking the contraction among W and two P_0 in the manner

$$P_{1\eta\xi}^{ab} = \sum_{d\zeta} W_{cde}^{ab} P_{0\eta\zeta}^{cd} P_{0\zeta\xi}^{de}, \quad (23)$$

we obtain the extended HCTM. It should be noted that one can choose arbitrary letter for the tensor legs, since they are just the dummy indices that are used for the contractions among tensors. By definition, $P_{1\eta\xi}^{ab}$ satisfies the left-right symmetry $P_{1\eta\xi}^{ab} = P_{1\xi\eta}^{ba}$. Similar to Eq. (23), the extension of the CTM at the bottom left corner is performed combining W , C_0 , and P_0 as

$$C_{1\xi}^{ab} = \sum_{cd\zeta} B_c^a W_{cde}^{ab} C_{0\zeta}^{cd} P_{0\zeta\xi}^{de}. \quad (24)$$

Figure 8 pictorially represents the extension processes in Eqs. (23) and (24). The extended CTM around the bottom

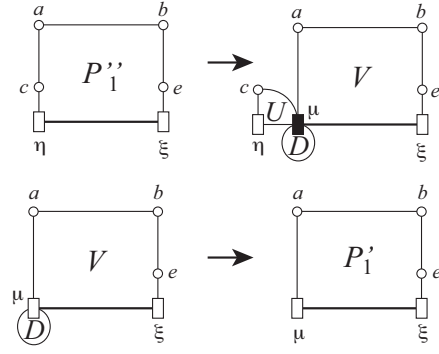


Fig. 9. The SVD in Eq. (25) and the basis transformation applied to the left side of $P_{1\eta\xi}^{ab}$ in Eq. (27).

right corner $C_{1\eta}^{ab}$ can be obtained in the same manner, but we do not have to explicitly calculate it, since the left-right symmetry of the lattice allows us to use $C_{1\eta}^{ab}$ in Eq. (24) also for the bottom right corner, after the appropriate substitution of indices.

We have put dash marks on $P_{1\eta\xi}^{ab}$ and $C_{1\eta}^{ab}$ in order to indicate that they have more tensor legs, respectively, compared with P_0 and C_0 . It is better to represent the pair of legs c and η , and also the pair e and ξ by something like block spin variables. For this purpose, we first divide the legs of $P_{1\eta\xi}^{ab}$ to the pair $c\eta$ and the rest, and then perform SVD

$$P_{1\eta\xi}^{ab} = \sum_{\mu} U_{\eta\mu}^c D_{\mu} V_{\mu\xi}^{ab}, \quad (25)$$

where D_{μ} denotes the singular values. We assume the decreasing order for D_{μ} with respect to μ . The SVD we have performed is pictorially shown in the upper part of Fig. 9.

The 3-leg tensor $U_{\eta\mu}^c$ in Eq. (25) satisfies the orthogonality

$$\sum_{c\eta} U_{\eta\mu}^c U_{\eta\mu'}^c = \delta_{\mu\mu'}, \quad (26)$$

which enables us to use it as the basis transformation. Let us apply it on $P_{1\eta\xi}^{ab}$ in the manner

$$\sum_{c\eta} U_{\eta\mu}^c P_{1\eta\xi}^{ab} = \sum_{c\eta} U_{\eta\mu}^c \sum_{\nu} U_{\eta\nu}^c D_{\nu} V_{\nu\xi}^{ab} = D_{\mu} V_{\mu\xi}^{ab} \quad (27)$$

from the left side, and express $D_{\mu} V_{\mu\xi}^{ab}$ by the new notation $P_{1\mu\xi}^{ab}$. We pictorially show the result of basis transformation in the lower part of Fig. 9. The left-right symmetry in $P_{1\eta\xi}^{ab}$ allows us to apply U to the right side of $P_{1\eta\xi}^{ab}$ and also to $P_{1\eta\xi}^{ab}$. For the latter, the transformation is performed as

$$\sum_{e\xi} P_{1\mu\xi}^{ab} U_{\xi\rho}^e = P_{1\mu\rho}^{ab} \quad (28)$$

to obtain the 4-leg tensor $P_{1\mu\rho}^{ab}$. The transformation U can be applied to $C_{1\xi}^{ab}$ in Eq. (24) from the right side, since the lattice structure around the legs b , e , and ξ is in common, as shown in Fig. 8. Performing the transformation

$$\sum_{e\xi} C_{1\xi}^{ab} U_{\xi\rho}^e = C_{1\rho}^{ab}, \quad (29)$$

we obtain the 3-leg tensor $C_{1\rho}^{ab}$. Figure 10 pictorially shows

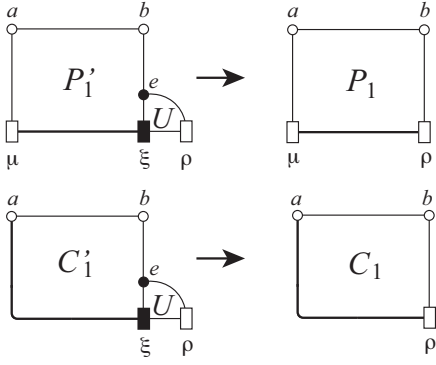


Fig. 10. The basis transformations applied to the right side of P'_1 in Eq. (28), and that of C'_1 in Eq. (29).

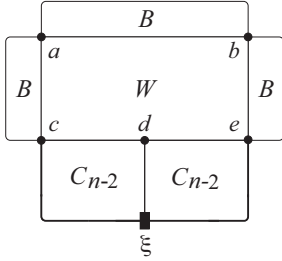


Fig. 11. The pictorial representation of $Z_n(T)$ in Eq. (30).

the transformations in Eqs. (28) and (29).

Initially we had P_0 in Eq. (20) and C_0 in Eqs. (21) and (22). Through the extension processes in Eqs. (23) and (24) and the basis transformations in Eqs. (27)-(29), we have obtained P_1 and C_1 . It is possible to repeat the extensions and the transformations again to obtain P_2 and C_2 . In this manner, we can construct the series of HCTMs P_0, P_1, P_2, \dots , and that of CTMs C_0, C_1, C_2, \dots . Every time we perform the basis transformation, the degree of freedom of the greek indices becomes twice. This exponential increase of the freedom can be avoided by discarding tiny singular values, and keeping only χ numbers of relevant basis in the transformations in Eqs. (27)-(29), which can be regarded as the RG transformations.

We can obtain spin expectation values by means of the contraction of the tensors we have obtained. First of all, the partition function in Eq. (2) is calculated as

$$Z_n(T) = \sum_{abcde\xi} B_{ab} B_c^a W_{cde}^{ab} B_e^b C_{n-2}^{cd} C_{n-2}^{de} \xi, \quad (30)$$

where the pictorial representation is shown in Fig. 11. The spin a at the top is σ_0^0 in previous notation, thus its expectation value is expressed as

$$\langle \sigma_0^0 \rangle = \sum_{abcde\xi} \frac{a}{Z_n(T)} B_{ab} B_c^a W_{cde}^{ab} B_e^b C_{n-2}^{cd} C_{n-2}^{de} \xi, \quad (31)$$

which is equal to $\langle \sigma_1^0 \rangle$. Rigorously speaking, the expectation value $\langle \sigma_0^0 \rangle$ is zero when the number of layers n is finite. Below the symmetry breaking temperature T_2 of the bulk in the thermodynamic limit, however, numerically obtained $\langle \sigma_0^0 \rangle$ and $\langle \sigma_1^0 \rangle$ becomes finite when n is sufficiently large, since tiny numerical errors, which are common in floating point arith-

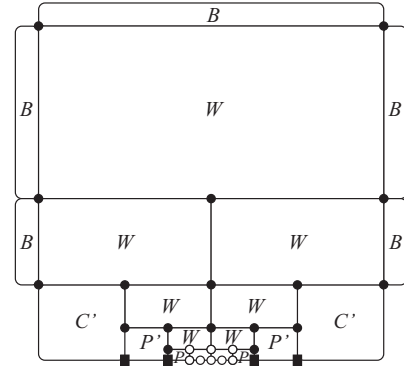


Fig. 12. The tensor E_{defghi}^{abc} used for the evaluation of $\langle \sigma_{m(5)/2}^5 \rangle = \langle \sigma_{16}^5 \rangle$. The tensor legs are denoted by open circles.

metics, slightly break the spin inversion symmetry. Alternatively we can impose a tiny external magnetic field h to the spins on the surface $\{\sigma^n\}$ to break the symmetry in a controlled manner.

In case we do not need the value of $Z_n(T)$ directly, we can multiply arbitrary factor to any tensors, since the factor cancels when we calculate the expectation values such as $\langle \sigma_0^0 \rangle$ in Eq. (31). Often the normalization of each tensor is performed so that the maximal absolute value of the element becomes unity, for the purpose of stabilize the floating-point arithmetics.

Combining all the tensors created up to the n -th iteration in the modified CTMRG algorithm, we can obtain the expectation value $\langle \sigma_{m(n)/2}^n \rangle$ at the center of the bottom row. Figure 12 shows the structure of the tensor E_{defghi}^{abc} that is necessary for the calculation of $\langle \sigma_{m(5)/2}^5 \rangle = \langle \sigma_{16}^5 \rangle$. The 8-leg tensor is created from the contraction among B, W, P_0, P'_1 , and C'_2 , where all the tensor legs other than 8 legs shown by open circles on the lowest W are summed up. It is important to take the configuration sum partially from up side to down side, as we performed in Eq. (5), to suppress the computational time. The expectation value is then obtained as

$$\langle \sigma_{m(5)/2}^5 \rangle = \frac{\sum_{a-i} f E_{defghi}^{abc}}{\sum_{a-i} E_{defghi}^{abc}} = \sum_{a-i} \frac{f}{Z_5(T)} E_{defghi}^{abc}, \quad (32)$$

where the sum is taken over for all the legs. In the same manner, we can obtain $\langle \sigma_{m(n)/2}^n \rangle$ for arbitrary system size n . Also we can calculate the expectation values $\langle \sigma_{m(i)/2}^i \rangle$ from $i = 1$ to n , where $\sigma_{m(i)/2}^i$ are located vertically, arranging the tensors appropriately and performing the contractions. Below the symmetry breaking temperature on the surface T_1 , finite value is obtained for $\langle \sigma_{m(n)/2}^n \rangle$ when n is sufficiently large.

It is also possible to obtain spin expectation values and correlation functions, creating another set of HRTMs and CTMs, each of which contain one of the IRF weights $a W_{cde}^{ab}$, $b W_{cde}^{ab}$, $c W_{cde}^{ab}$, $d W_{cde}^{ab}$, and $e W_{cde}^{ab}$ at the specified location. In this case, an Ising spin is implicitly contained in the renormalized tensors. This approach is well known in the TRG formulations,^{41,42} and we calculate the end-to-end correlation function $\langle \sigma_0^n \sigma_{m(n)}^n \rangle$ by this approach.

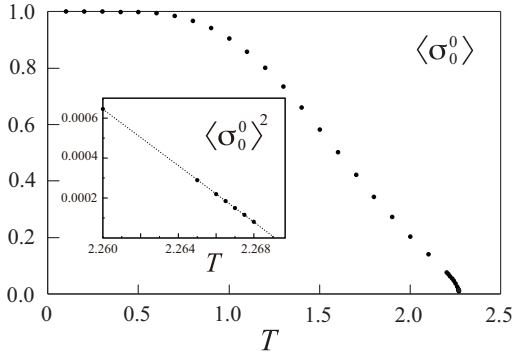


Fig. 13. Spontaneous magnetization $\langle \sigma_0^0 \rangle$ in the bulk. The square $\langle \sigma_0^0 \rangle^2$ is shown in the inset.

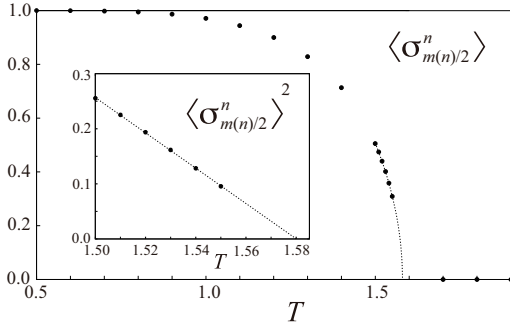


Fig. 14. Spontaneous magnetization $\langle \sigma_{m(n)/2}^n \rangle$ on the surface, when n is sufficiently large. The square $\langle \sigma_{m(n)/2}^n \rangle^2$ is shown in the inset.

3.1 Calculated Results by the Modified CTMRG Method

We perform the numerical calculation on the hierarchical pentagon lattice by means of the modified CTMRG method, keeping $\chi = 55$ degrees of freedom at most when we perform the RG transformation. The expectation value $\langle \sigma_{m(n)/2}^n \rangle$ is converged with respect to n less than $n = 100$ at any temperature. In case of $\langle \sigma_0^0 \rangle$, the convergence becomes slow near the transition temperature, and therefore we performed the iterative calculation up to $n = 30000$ at most. For all the data we show in this section, we checked the convergence with respect to χ and n .

Figure 13 shows the temperature dependence of the spontaneous magnetization $\langle \sigma_0^0 \rangle$ at the top, which are regarded as the bulk part of the system. Around $T = 1$, the plotted value decreases with T , as if it vanishes somewhere between $T = 1.5$ and $T = 2.0$. But the decreasing rate becomes almost constant around $T = 1.5$, and finally the value vanishes at the transition temperature $T_2 = 2.269$. As shown in the inset, $\langle \sigma_0^0 \rangle^2$ shows linear behavior near $T = T_2$. The behavior suggests that the transition is mean-field like, as it was observed in the bulk part of the hyperbolic lattices.^{20–24)}

Figure 14 shows the temperature dependence of $\langle \sigma_{m(n)/2}^n \rangle$ at the center of the bottom spin row, which are regarded as the surface of the system. As shown in the inset, the squared value $\langle \sigma_{m(n)/2}^n \rangle^2$ shows linear behavior around the transition temperature $T_1 = 1.58$. The dotted lines show the linear fitting result, and the corresponding dotted curve is also drawn for $\langle \sigma_{m(n)/2}^n \rangle$. The transition is again mean-field like. The curious behavior of $\langle \sigma_0^0 \rangle$ in Fig. 13 might be related to presence of the

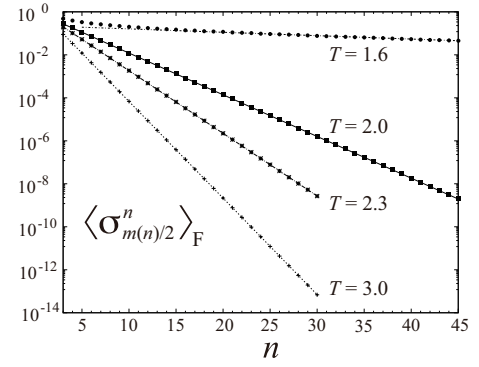


Fig. 15. Decay of $\langle \sigma_{m(n)/2}^n \rangle_F$ with respect to n .

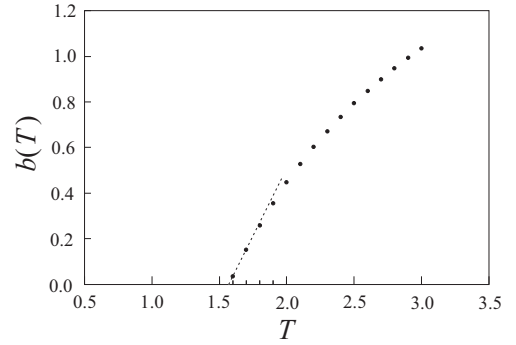


Fig. 16. Decay rate $b(T)$ in Eq. (33) with respect to T . The dotted line connects the plots at $T = 1.6$ and $T = 1.7$.

symmetry breaking on the surface at T_1 .

For the purpose of examining the value of T_1 by alternative view point, we observe the decay of spin correlation along the vertical direction. Let us impose the ferromagnetic boundary condition $\sigma_0^0 = \sigma_1^0 = 1$ at the top of the system, when we calculate the environment tensor E_{defghi}^{abcd} shown in Fig. 12. We denote the corresponding expectation value as $\langle \sigma_{m(n)/2}^n \rangle_F$. Below T_1 , we obtain the same value $\langle \sigma_{m(n)/2}^n \rangle = \langle \sigma_{m(n)/2}^n \rangle_F$ as the spontaneous magnetization, when n is sufficiently large. Above T_1 , $\langle \sigma_{m(n)/2}^n \rangle_F$ show exponential dumping with respect to n , as shown in Fig. 15. The dotted lines denote the linear fitting result in the region where the exponential dumping

$$\langle \sigma_{m(n)/2}^n \rangle_F \propto e^{-b(T)n} \quad (33)$$

is observed clearly, where $b(T)$ is the decay rate. Only in the case $T = 1.6$, several plots visibly deviate from the dotted line in the small n region. Figure 16 shows the temperature dependence of $b(T)$. No singular behavior is observed at the bulk transition temperature $T_2 = 2.269$, and $b(T)$ almost linearly decreases to zero at $T_1 = 1.58$. The result suggests that the spin correlation length to the vertical direction diverges at T_1 with the index $\nu = 1$, which is different from the mean-field value $\nu = 1/2$.

In the intermediate temperature region $T_1 < T < T_2$, the bulk spin has finite spontaneous magnetization as shown in Fig. 13, and the surface magnetization is absent as shown in Fig. 14. In order to capture the magnetization profile between these two parts, we calculate the expectation values of the vertically aligned spins $\langle \sigma_{m(i)/2}^i \rangle$ from $i = 1$ to $i = 150$ in the case

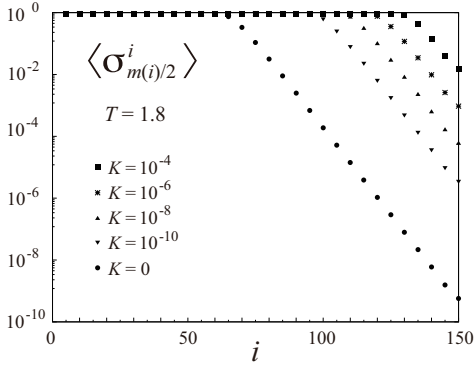


Fig. 17. The expectation values $\langle \sigma_{m(i)/2}^i \rangle$ from $i = 5$ to $i = 150$ that are calculated for the system with $n = 150$ layers when $T = 1.8$.

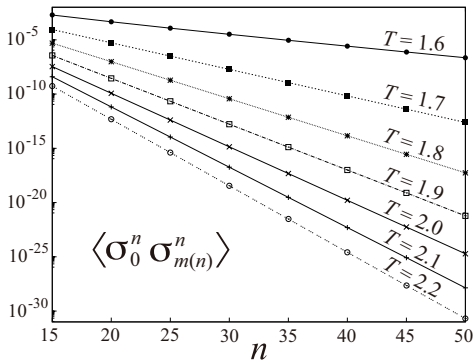


Fig. 18. Correlation function $\langle \sigma_0^n \sigma_{m(n)}^n \rangle$.

where the system contains $n = 150$ layers. In order to observe the symmetry breaking in a controlled manner, we impose a weak magnetic field h to the surface spins $\{\sigma^n\}$. The initial HCTM is then modified as

$$P_{0\ ce}^{ab} = \sum_d W_{cde}^{ab} B_{cd} B_{de} \exp\left[\frac{K}{2}(c + 2d + e)\right], \quad (34)$$

where the parameter $K = \mu_B h / k_B T$ represents the effect of the magnetic interaction with the Bohr moment μ_B . Similarly, the initial CTM is modified as

$$C_{0\ e}^{ab} = \sum_{cd} B_c^a W_{cde}^{ab} B_{cd} B_{de} \exp\left[\frac{K}{2}(2c + 2d + e)\right]. \quad (35)$$

We perform the calculation for the cases where $K = 10^{-4}, 10^{-6}, 10^{-8}, 10^{-10}$, and 0. Figure 17 shows the calculated $\langle \sigma_{m(i)/2}^i \rangle$ from $i = 5$ to $i = 150$ when $T = 1.8$. Exponential dumping with respect to i is clearly observed near the surface, and the dumping rate is consistent with $b(T = 1.8)$ obtained from the plots at $T = 1.8$ in Fig. 15. In the case $K = 0$, the surface magnetization $\langle \sigma_{m(150)/2}^{150} \rangle$ is *artificially induced* by a tiny numerical error. The magnetic profiles plotted in Fig. 17 shows that there is a polarized area in the bulk part. The situation is common to the Ising model on the Cayley tree below the bulk symmetry breaking temperature.

Finally, let us examine how strongly σ_0^n and $\sigma_{m(n)}^n$ are correlated, observing the expectation value $\langle \sigma_0^n \sigma_{m(n)}^n \rangle$ for the zero field case $K = 0$. Figure 18 shows the calculated result from $T = 1.6$ to $T = 2.2$ by the step $\Delta T = 0.1$, with respect to n .

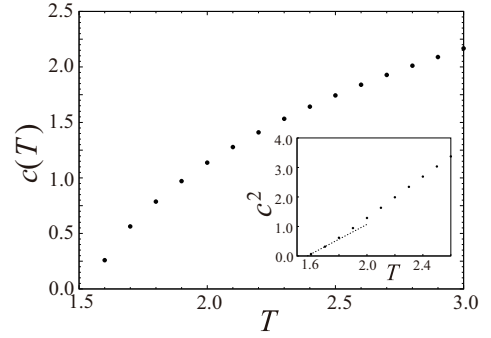


Fig. 19. Temperature dependence of the exponent $c(T)$ in Eq. (36). We show the square $[c(T)]^2$ in the inset.

The exponential dumping

$$\langle \sigma_0^n \sigma_{m(n)}^n \rangle \propto e^{-c(T)n} \quad (36)$$

is clearly observed, where $c(T)$ is the dumping constant. It should be noted that the distance ℓ between σ_0^n and $\sigma_{m(n)}^n$ measured along the surface is $m(n) = 2^n$. From the relation

$$\ell^{-\eta} = (2^n)^{-\eta} \propto e^{-c(T)n}, \quad (37)$$

the exponent for the power-law decay along the surface is estimated as

$$\eta = \frac{c(T)}{\ln 2}. \quad (38)$$

Figure 19 shows the temperature dependence of $c(T)$. Squared values $[c(T)]^2$ shown in the inset are nearly proportional to $T - T_1$ near $T = T_1$. If we draw the line that passes the plots $[c(1.6)]^2$ and $[c(1.7)]^2$ in the inset, we obtain $T_1 = 1.58$ again. Considering the fact that the shortest path from σ_0^n to $\sigma_{m(n)}^n$ is $2n + 1$, it is expected that $c(T)$ in Eq. (36) is nearly twice as large as $b(T)$ in Eq. (33). Comparing Fig. 16 and Fig. 19, one finds that the relation $c(3.0) \sim 2b(3.0)$ is satisfied, where the correlation length to the vertical direction is short at this temperature. Near $T = T_1$, when the correlation length is long, the relation does not hold any more. From the value of $c(T)$ at $T = 2.4, 2.6, 2.8$, and 3.0 , we calculate η by Eq. (38), and draw the corresponding lines in Fig. 5. Qualitative agreement is observed about the decay rate estimated from the TEBD method and that from the modified CTMRG method.

4. Conclusions and Discussions

We numerically observed the phase transition of the Ising model on the hierarchical pentagon lattice, by means of the tensor network methods. By means of the TEBD method up to the number of layers $n = 10$, the distribution function G_n on the surface is calculated. The corresponding entanglement entropy $S(T)$ with respect to the bipartition of the surface spin row shows peak structure, whose height increases with n . In the high temperature region $T \geq 2.4$, the power-law decay of the correlation function along the surface is observed. By means of the modified CTMRG method, the bulk transition of the mean-field type is detected at $T_2 = 2.269$, at the top of the system. On the surface, which is the spin row at the bottom, the order-disorder transition of the mean-field type is detected at $T_1 = 1.58$, which is lower than T_2 . The end-to-end correlation function $\langle \sigma_0^n \sigma_{m(n)}^n \rangle$ shows exponential dumping with n above T_1 , which agrees with the power-law decay of the spin

correlation function observed by the TEBD method.

Contrary to the thermodynamics on the Cayley tree, we observed the phase transition on the surface, which is the outer system boundary, below T_1 . This difference can be explained by the presence of loops in hierarchical pentagon lattice. It should be noted that the surface spin row $\{\sigma^n\}$ can be regarded as the one-dimensional Ising model, where upper layers effectively induce long-range interactions. The similar structure is present also in hyperbolic (p, q) lattices, and therefore phase transition could be present on the boundary in these hyperbolic lattices.

The hierarchical pentagon lattice we treated in this article can be considered as a fractal lattice, in the sense that it has self similarity. On the fractal lattice such as the Sierpinski carpet, it is known that the critical behavior is highly dependent on the location of the site in the system.^{39,40} Thus the possible coming study is to observe spin expectation values $\langle \sigma_j^i \rangle$ and correlation functions $\langle \sigma_j^i \sigma_k^\ell \rangle$ for a various combination of i, j, k , and ℓ . In principle, it is at least possible to target arbitrary pair of spins from the row spins $\{\sigma^n\}$ on the surface, and obtain expectation values such as $\langle \sigma_j^i \rangle$ and $\langle \sigma_j^i \sigma_\ell^n \rangle$ for arbitrary j and ℓ . To construct a systematic numerical algorithm, which automatically choose the necessary pieces of tensors for the targetted spins, is one of the next computational challenge in the modified CTMRG method, which has many aspects in common with the tensor renormalization group (TRG)^{41,42} studies.

In the application of the TEBD method, every time we multiply the transfer matrix, the number of 3-leg tensor contained in the MPS representation of G_n becomes almost twice. This is the reason why our TEBD calculation is limited up to $n = 10$. In the case when we are only interested in the region around the center of the surface spin row, we can ignore those 3-leg tensors that are located near the left and right boundary of the row, and can *shrink* the length of MPS. Such an approximation is possible in the case where the surface area extension is more rapid than the propagation of correlation effect. Such a numerical trick is similar to the tensor eliminations in the co-moving MPS window method,^{43,44} performed in the back side of the window.

T.N. was supported by JSPS KAKENHI Grant Number 21K03403 and by the COE research grant in computational science from Hyogo Prefecture and Kobe City through Foundation for Computational Science. We thank to valuable discussions with K. Okunishi and H. Ueda.

1) L.P. Kadanoff, *Statistical Physics: Statics, Dynamics, and Renormalization*, World Scientific, Singapore (2000).

2) E. Ising, *Z. Phys.* **31**, 253 (1925).

3) S.G. Brush, *Rev. Mod. Phys.* **39**, 883 (1967).

4) R. Peierls, in *Mathematical Proceedings of the Cambridge Philosophical Society*, vol. **32**, 477, (1936).

- 5) L. Onsager, *Phys. Rev.* **65**, 117 (1944).
- 6) L.P. Kadanoff, *Physics* **2**, 263 (1966).
- 7) E. Efrati, Z. Wang, A. Kolan, L.P. Kadanoff, *Rev. Mod. Phys.* **86**, 647 (2014).
- 8) K. Wilson and J. Kogut, *Phys. Rep.* **12**, 75 (1974).
- 9) A.A. Belavin, A.M. Polyakov, A.B. Zamolodchikov, *Nuclear Phys. B.* **241**, 333 (1984).
- 10) R.J. Baxter, *Exactly Solved Models in Statistical Mechanics*, Academic press, (1989); Dover Publications (2008).
- 11) L.K. Runnels, *J. Math. Phys.* **8**, 2081 (1967).
- 12) T.P. Eggarter, *Phys. Rev. B* **9**, 2989 (1974).
- 13) E. Müller-Hartmann, and J. Zittartz, *Phys. Rev. Lett.* **33** 893 (1974).
- 14) H.A. Bethe, *Proc. Roy. Soc. London A* **150**, 552 (1935).
- 15) R.J. Baxter, *J. Math. Phys.* **9**, 650 (1968).
- 16) R.J. Baxter, *J. Stat. Phys.* **19**, 461 (1978).
- 17) T. Nishino, and K. Okunishi, *J. Phys. Soc. Jpn.* **65**, 891 (1996).
- 18) T. Nishino, and K. Okunishi, *J. Phys. Soc. Jpn.* **66**, 3040 (1997).
- 19) R. Orus, and G. Vidal, *Phys. Rev. B* **80**, 094403 (2009).
- 20) K. Ueda, R. Krčmar, A. Gendiar, and T. Nishino, *J. Phys. Soc. Jpn.* **76**, 084004 (2007).
- 21) R. Krčmar, A. Gendiar, K. Ueda, and T. Nishino, *J. Phys. A: Math. Theor.* **41**, 215001 (2008).
- 22) A. Gendiar, M. Daniska, R. Krčmar, and T. Nishino, *Phys. Rev. E* **90**, 012122 (2014).
- 23) T. Iharagi, A. Gendiar, H. Ueda, and T. Nishino, *J. Phys. Soc. Jpn.* **79**, 104001 (2010).
- 24) A. Gendiar, R. Krčmar, S. Andergassen, M. Daniska, and T. Nishino, *Phys. Rev. E* **86**, 021105 (2012).
- 25) M. Asaduzzaman, Simon Catterall, Jay Hubisz, Roice Nelson, and Judah Unmuth-Yockey, *Phys. Rev. D* **106**, 054506 (2022).
- 26) K. Okunishi, and T. Takayanagi, *Prog. Theor. Exp. Phys.* **013A03** (2024).
- 27) J.M. Maldacena, *Adv. Theor. Math. Phys.* **2**, 231 (1998).
- 28) S. Gubser, I. Klebanov, and A. Polyakov, *Physics Lett. B* **428**, 105 (1998).
- 29) E. Witten, *Adv. Theor. Math. Phys.* **2**, 253 (1998).
- 30) O. Aharony, S.S. Gubser, J.M. Maldacena, H. Ooguri, and Y. Oz, *Phys. Rept.* **323**, 183 (2000).
- 31) G. Vidal, *Phys. Rev. Lett.* **93**, 040502 (2004).
- 32) S. R. White and A. E. Feiguin, *Phys. Rev. Lett.* **93**, 076401 (2004).
- 33) G. Vidal, *Phys. Rev. Lett.* **101**, 110501 (2008).
- 34) G. Evenbly, and G. Vidal, *Phys. Rev. B* **79**, 144108 (2009).
- 35) S. Ostlund, and S. Rommer, *Phys. Rev. Lett.* **75**, 3537 (1995).
- 36) U. Schollwöck, *Annals of Physics* **326**, 96 (2011).
- 37) When we consider the tensor legs a, b, c, d and e as the Ising spins, they take the value either 1 or -1 . In the computational programing, they are treated as bits, that take either 0 or 1.
- 38) The IRF-type tensor network diagram invented by Baxter^{10,16} is convenient when the system is represented as the IRF model, which contains Ising and Potts models on the planer lattice.
- 39) J. Genzor, A. Gendiar, and T. Nishino, *Phys. Rev. E* **93**, 012141 (2016).
- 40) J. Genzor, A. Gendiar, and T. Nishino, *Phys. Rev. E* **107**, 044108 (2023).
- 41) M. Levin, and C.P. Nave, *Phys. Rev. Lett.* **99**, 120601 (2007).
- 42) Z.Y. Xie, J. Chen, M.P. Qin, J.W. Zhu, L.P. Yang, and T. Xiang, *Phys. Rev. B* **86**, 045139 (2012).
- 43) H.N. Phien, G. Vidal, and I.P. McCulloch, *Phys. Rev. B* **86**, 245107 (2012).
- 44) V. Zauner, M. Ganahl, H.G. Everts, and T. Nishino, *J. Phys.: Condens. Matter* **27**, 425602 (2015).